Preprints.org

Article

Not peer-reviewed version

Synthesis-Dependent Adsorption Properties of Polythioamides Toward Mercury(II) Ions

Yue Gao *, Cheng Ma *, Xuan Qi *, Hao Yan *, Chao Yang, Wei Xia, Hanyu Du, Junfeng Zhang

Posted Date: 25 November 2025

doi: 10.20944/preprints202511.1916.v1

Keywords: polythioamides; multicomponent polymerization (MCP); elemental sulfur utilization; mercury(II) adsorption; environmental remediation

Preprints.org is a free multidisciplinary platform providing preprint service that is dedicated to making early versions of research outputs permanently available and citable. Preprints posted at Preprints.org appear in Web of Science, Crossref, Google Scholar, Scilit, Europe PMC.

Copyright: This open access article is published under a Creative Commons CC BY 4.0 license, which permit the free download, distribution, and reuse, provided that the author and preprint are cited in any reuse.

Preprints.org (www.preprints.org) | NOT PEER-REVIEWED | Posted: 25 November 2025 doi:10.20944/preprints202511.1916.v1

Disclaimer/Publisher's Note: The statements, opinions, and data contained in all publications are solely those of the individual author(s) and contributor(s) and not of MDPI and/or the editor(s). MDPI and/or the editor(s) disclaim responsibility for any injury to people or property resulting from any ideas, methods, instructions, or products referred to in the content.

Article

Synthesis-Dependent Adsorption Properties of Polythioamides Toward Mercury(II) Ions

Yue Gao [1,*], Cheng Ma [2,*], Xuan Qi [1,*], Hao Yan [1,*], Chao Yang [3], Wei Xia [1], Hanyu Du [2] and Junfeng Zhang [4]

[1] College of Chemical and Materials Engineering, Hainan vocational University of Science and Technology, Hainan 571126, China

[2] School of Petrchemical Engineering, Liaoning Petrochemical University, Fushun 113001, China

[3] SINOPEC Dalian Research Institute of Petrochemical Technology, Dalian 116000, China

[4] School of Chemistry and Chemical Engineering, Hainan University, China

* Correspondence: yueyuezcs@163.com (Y.G.); kkmc2002@163.com (C.M.); 7duan@163.com (X.Q.); yanhao0898@126.com (C.Y.)

Abstract

Sulfur is an important constant element in the crust, with a mass abundance of approximately 0.03%, is mainly obtained as a by-product of hydrodesulfurization in petroleum refining. Although China produces over ten million tons of sulfur annually, its applications remain limited, and while sulfur is not flammable under normal conditions, its oxidizability and potential to catch fire under extreme conditions pose safety and environmental risks during storage. To address these issues, we developed a multicomponent polymerization (MCP) strategy using elemental sulfur, dicarboxylic acids, and diamines to synthesize functional polythioamides. This metal-free approach utilizes readily available raw materials and enables the efficient construction of structurally diverse polymers. Unlike previously reported MCP systems relying on aromatic monomers, our work employed aliphatic diamines and diacids, yielding polythioamides with rigid structures and excellent properties. Characterization by Fourier-transform infrared spectroscopy (FT-IR), thermogravimetric analysis (TGA), X-ray photoelectron spectroscopy (XPS). Adsorption studies demonstrated a strong affinity for Hg(II), with a maximum capacity of 187 $mg \cdot g^{-1}$. SEM, XPS revealed clear morphological and compositional changes after Hg(II) uptake, confirming efficient adsorption. This work highlights MCP as a promising route for converting sulfur into functional polymers with high potential in wastewater treatment and environmental remediation.

Keywords: polythioamides; multicomponent polymerization (MCP); elemental sulfur utilization; mercury(Ⅱ) adsorption; environmental remediation

1. Introduction

Sulfur is an important constant element in the crust, with a mass abundance of approximately 0.03%. It is primarily obtained as a by-product of hydrodesulfurization in petroleum refining. In China alone, more than ten million tons of sulfur are produced annually. However, despite its high yield, sulfur suffers from limited applications, and its inherent flammability and oxidizability present significant safety and environmental risks during storage [1–3]. The development of effective strategies to convert this underutilized resource into value-added materials has therefore attracted considerable attention.

Sulfur-containing polymers, particularly those synthesized through Inverse Vulcanization, have emerged as a promising class of materials due to their unique chemical and physical properties [4]. Recent studies have focused on enhancing the properties and applications of sulfur-containing polymers, particularly through the exploration of alternative synthesis techniques. One of the most significant innovations is the use of Inverse Vulcanization, which allows the incorporation of sulfur

© 2025 by the author(s). Distributed under a Creative Commons CC BY license.

Preprints.org (www.preprints.org) | NOT PEER-REVIEWED | Posted: 25 November 2025 doi:10.20944/preprints202511.1916.v1

into polymer backbones, resulting in materials with improved thermal stability, conductivity, and mechanical strength. However, challenges remain in controlling the structural and functional diversity of these materials. Additionally, the scalability and efficiency of synthesis methods are key barriers to their broader adoption in industrial applications. Recent efforts have sought to address these issues by exploring metal-free polymerization systems, which avoid the use of toxic or expensive transition-metal catalysts [5]. This approach has been shown to improve the sustainability and cost-effectiveness of sulfur polymer production. Nevertheless, there remains a significant gap in developing metal-free multicomponent polymerization (MCP) systems that can efficiently integrate sulfur, aliphatic diamines, and dicarboxylic acids into structurally diverse polymers. Such polymers could offer enhanced mechanical properties, improved thermal stability, and novel functionalization possibilities, which are critical for the expansion of their applications in areas such as environmental remediation, energy storage, and industrial coatings [6]. These polymers play important roles in diverse applications, including energy storage devices such as lithium – sulfur batteries, ion sensors, heavy-metal adsorption, high-temperature and corrosion-resistant materials, and self-healing systems [7,8]. Polythioamides, a subclass of sulfur-containing polymers, are notable for their strong sulfur – metal interactions, excellent thermal stability, and versatile functionalization potential, making them attractive candidates for both environmental and industrial applications [9–12].

Recent advances in the synthesis of sulfur-containing polymers have led to the development of multicomponent polymerization (MCP) as a powerful and efficient synthetic strategy for constructing such materials [13–16]. MCP offers several advantages, including simplicity, high reactivity, and the ability to generate structural diversity without the need for transition-metal catalysts. While most reported MCP systems employ aromatic diamines and diacids as monomers, the exploration of aliphatic monomers remains limited [17–19]. The incorporation of aliphatic diamines and diacids into MCP could offer the potential for preparing polythioamides with distinct rigid structures and enhanced properties.

Despite the growing interest in sulfur-based polymers, a gap remains in the systematic exploration of metal-free MCP systems that can incorporate elemental sulfur, aliphatic diamines, and dicarboxylic acids. Addressing this gap, we developed a metal-free MCP system to synthesize functional polythioamides. The polymer structures and thermal stability were systematically characterized by Fourier-transform infrared spectroscopy (FT-IR), thermogravimetric analysis (TGA), and X-ray photoelectron spectroscopy (XPS). Furthermore, the Hg(II) adsorption capacity by the developed polythioamides was investigated under various conditions [20–24]. After the adsorption experiments, SEM, and XPS analyses were conducted to confirm the effective uptake of Hg(II) into the synthesized polythioamides. This study not only demonstrates an efficient strategy for the valorization of elemental sulfur but also introduces a class of functional polymers with significant potential in wastewater treatment and environmental remediation.

2. Results and Discussion

2.1. FTIR Analysis

The two monomers and the resulting polythioamides were characterized by Fourier-transform infrared (FT-IR) spectroscopy (Figure 1a). The absorption peak at 2852 cm^{-1} corresponds to the C–H stretching vibration of methylene groups [25]. A comparison between the spectrum of adipic acid and that of polymer P1 shows that the C=O stretching vibration peak of adipic acid at 1698 cm^{-1} [26]. Disappears in the spectrum of P1, indicating complete monomer consumption. In the case of hexamethylenediamine, the $–NH_2$ absorption band at 3323 cm^{-1} shifts to a –NH– absorption peak at 3416 cm^{-1} in polymer P1, confirming the formation of thioamide groups.

3419 cm^{-1} and 3323 cm^{-1}: These peaks are attributed to the N–H stretching vibrations of the amide groups in the polymer. The peak at 3419 cm^{-1} corresponds to the free amine group ($–NH_2$), while the peak at 3323 cm^{-1} is due to the –NH– group formed during polymerization. These bands are typical for amides and indicate the presence of the N–H functional groups in the polythioamide structure.

© 2025 by the author(s). Distributed under a Creative Commons CC BY license.

Preprints.org (www.preprints.org) | NOT PEER-REVIEWED | Posted: 25 November 2025 doi:10.20944/preprints202511.1916.v1

1639 cm^{-1} and 1678 cm^{-1}: These peaks are attributed to the C=O stretching vibrations of the carbonyl groups. Specifically, the peak at 1639 cm^{-1} is associated with the carbonyl stretching of the amide group (C=O), while the peak at 1678 cm^{-1} corresponds to the C=O stretch of the original monomeric components that have been incorporated into the polymer.

The C=S stretching vibration, a characteristic feature of the thioamide group, typically appears in the range of ~1050–1250 cm^{-1}. The peaks observed at 1639–1678 cm^{-1} are attributed to the C=O stretch, which further supports the successful polymerization of the thioamide structures.

For all 26 synthesized polymers, the –NH– stretching vibration peaks appeared within the range of 3190–3464 cm^{-1}. Notably, in polymers P17–P21, characteristic absorption peaks of –NH– and C=S were observed at 3200–3460 cm^{-1} and 1605–1649 cm^{-1}, respectively. The presence of these peaks provides strong evidence for the successful formation of the polythioamide structures [27,28].

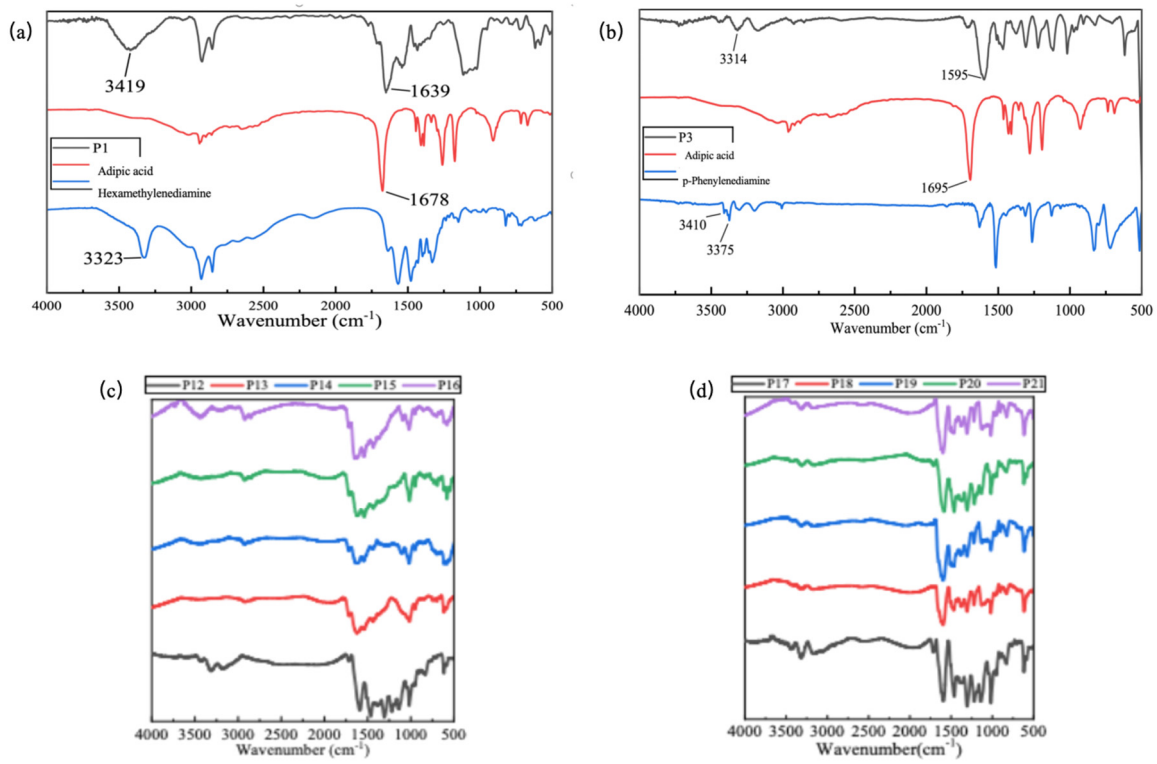

Figure 1. Infrared spectra of (a) aliphatic polythioamide and its raw materials. (b) aromatic polythioamide and its raw materials. (c) aliphatic polythiamide and (d) aromatic polythioamide.

Similarly, in the FT-IR spectrum of the aromatic product P3 (Figure 1b), the characteristic peak at 3000 cm^{-1} corresponds to the C–H stretching vibration of the benzene ring, while the absorption bands between 2800 and 3000 cm^{-1} are attributed to the stretching vibrations of saturated C–H bonds. In addition, the $–NH_2$ doublet of the p-phenylenediamine monomer at 3410 and 3375 cm^{-1} undergoes a significant change in polymer P3, converting into a single –NH– absorption peak at 3314 cm^{-1}. Moreover, a newly emerged peak at 1595 cm^{-1} can be clearly assigned to the C=S stretching vibration of the thioamide group.

These spectral changes provide strong evidence that the monomers were fully incorporated into the polymerization, leading to the successful formation of polymer P3 with characteristic thioamide structures.

Furthermore, a comparison between the spectra of aliphatic and aromatic polythioamides (Figure 1c,d) shows consistent results. Specifically, P12–P16 correspond to aliphatic polythioamides, while P17–P21 are aromatic polythioamides. In both cases, the characteristic peaks of the starting acids and amines disappeared, replaced by the C=S stretching vibration at 1580–1605 cm^{-1} and the –

© 2025 by the author(s). Distributed under a Creative Commons CC BY license.

Preprints.org (www.preprints.org) | NOT PEER-REVIEWED | Posted: 25 November 2025 doi:10.20944/preprints202511.1916.v1

NH– stretching vibration at 3183–3439 cm^{-1}. This confirms that regardless of the type of diamine or diacid used, the MCP process successfully yielded polythioamide structures with distinct thioamide signatures.

2.2. XRD Analysis

During the reaction at 100 °C, the synthesized polymers undergo a crystalline-to-amorphous transition (Figure 2). Using P3 and P17 as representative examples, their XRD patterns evolve from sharp reflections characteristic of elemental sulfur to broad, diffuse halos. In crystalline orthorhombic sulfur (S_8), strong Bragg peaks are typically observed near $2\theta \approx 23–24°$ (along with reflections at ~25.9°, 26.8°, 27.9°, 28.8°, and 31.4°), reflecting its well-ordered lattice [29,30]. By contrast, the prominent ~23° peak evident in the sulfur reference is absent in polymers P3 and P17, and the diffractograms display an amorphous halo, indicating the loss of long-range order and the chemical incorporation of sulfur into the polymer network rather than simple physical blending. This disappearance of crystalline sulfur peaks and the emergence of an amorphous pattern are consistent with prior observations in sulfur-rich polymer systems, where XRD confirms the conversion of crystalline sulfur into amorphous, chemically cross-linked frameworks [31,32]. Moreover, recent studies on carbon–sulfur composites and sulfur-based polymers similarly report that sulfur becomes X-ray amorphous upon effective integration into organic matrices, reinforcing our assignment of chemically bonded sulfur in the present materials [33,34].

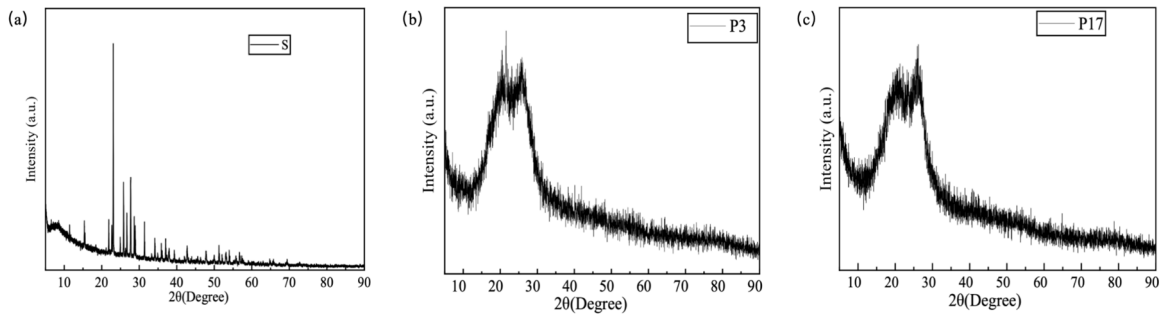

Figure 2. XRD pattern of (a) elemental S (b) polythioamide P3 (c) polythioamide P17.

2.3. SEM Analysis

As shown in the SEM images of polysulfamides (Figure 3), the aliphatic polysulfamide displays a relatively smooth and homogeneous surface, whereas the aromatic polysulfamide exhibits a rough and uneven morphology. This contrast suggests that the introduction of aromatic structures may induce surface irregularities, likely due to differences in chain packing density and intermolecular interactions.

As shown in (Figure 4), the EDS characterization results reveal the elemental compositions of the selected products. Specifically, P1 and P13 correspond to aliphatic polysulfamides, while P3 and P4 are aromatic polysulfamides. The sulfur content of both types falls within a comparable range of 20–35 wt%, indicating no substantial differences between them. This similarity suggests that the polymerization method exhibits strong universality, as it enables the efficient synthesis of target polysulfamides from both aliphatic and aromatic monomers. The comparable sulfur incorporation further implies that the reactivity of the monomers is not significantly affected by the presence of aromatic groups, highlighting the robustness of the polymerization strategy.

© 2025 by the author(s). Distributed under a Creative Commons CC BY license.

Preprints.org (www.preprints.org) | NOT PEER-REVIEWED | Posted: 25 November 2025 doi:10.20944/preprints202511.1916.v1

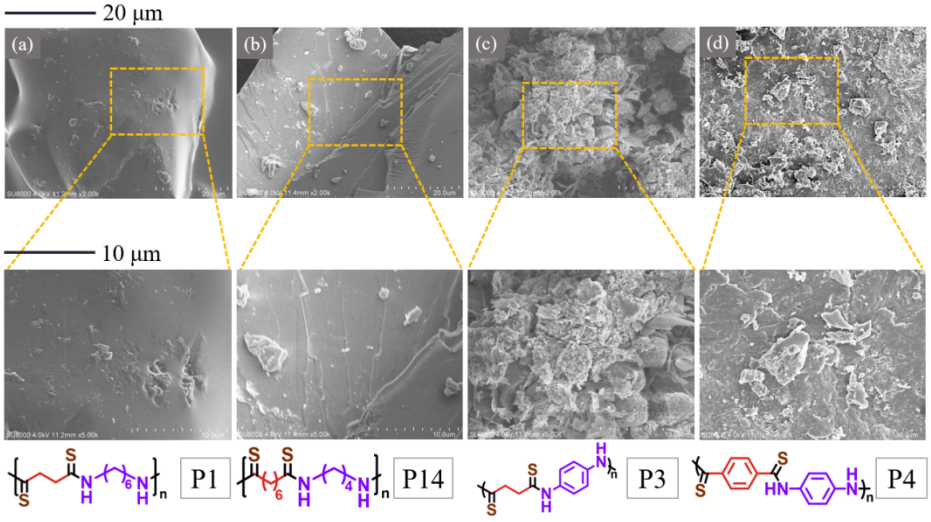

Figure 3. SEM images of P1, P14, P3, P4, and their corresponding magnified images.

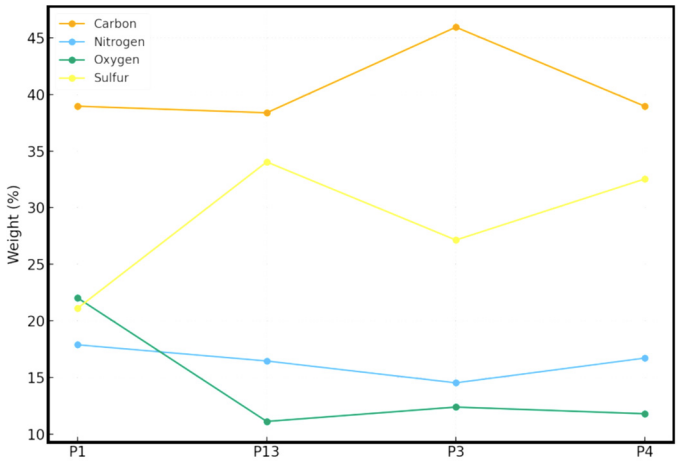

Figure 4. Quantitative elemental analysis results of polythioamide.

2.4. XPS Analysis

X-ray photoelectron spectroscopy (XPS) was employed to further elucidate the chemical structures of the synthesized polythioamides (Figure 5) [35–37]. Elemental sulfur, an aliphatic polysulfonamide (P26), and aromatic polythioamides (P4, P17, and P18) were analyzed by S 2p orbital scanning. The obtained spectra revealed that elemental sulfur exhibited binding energies at 164.30 and 165.5 eV. In comparison, the binding energies of sulfur in P26, P4, P17, and P20 were 164.00/164.95 eV, 163.85/165.05 eV, 163.65/164.7 eV, and 163.55/164.65 eV, respectively.

These observations confirm the presence of sulfur atoms in the polymers, with similar chemical environments across P4, P17, and P18. However, the distinct binding energy shifts compared with elemental sulfur indicate altered bonding states, suggesting the absence of unreacted sulfur. Moreover, the lower binding energies of sulfur in the products imply coordination with atoms of lower electronegativity. Corroborating evidence was obtained from infrared spectroscopy (Figure 5), where the characteristic C=O stretching band of carboxylic acid either disappeared or weakened, accompanied by the emergence of a new absorption peak at 1595 cm^{-1}. This strongly supports the incorporation of C=S functional groups within the polymer backbone.

Interestingly, a correlation was observed between the chain length of the repeating units and the binding energy shift of sulfur in the C=S bonds. The deviations from elemental sulfur were more pronounced for longer-chain polythioamides, as exemplified by ΔE17 = 0.65/0.8 eV and ΔE20 =

© 2025 by the author(s). Distributed under a Creative Commons CC BY license.

Preprints.org (www.preprints.org) | NOT PEER-REVIEWED | Posted: 25 November 2025 doi:10.20944/preprints202511.1916.v1

0.75/0.85 eV. This trend suggests that elongation of the repeating unit enhances the localization of electron density on the sulfur atom within the C=S bond, which may have implications for the electronic properties of the resulting materials.

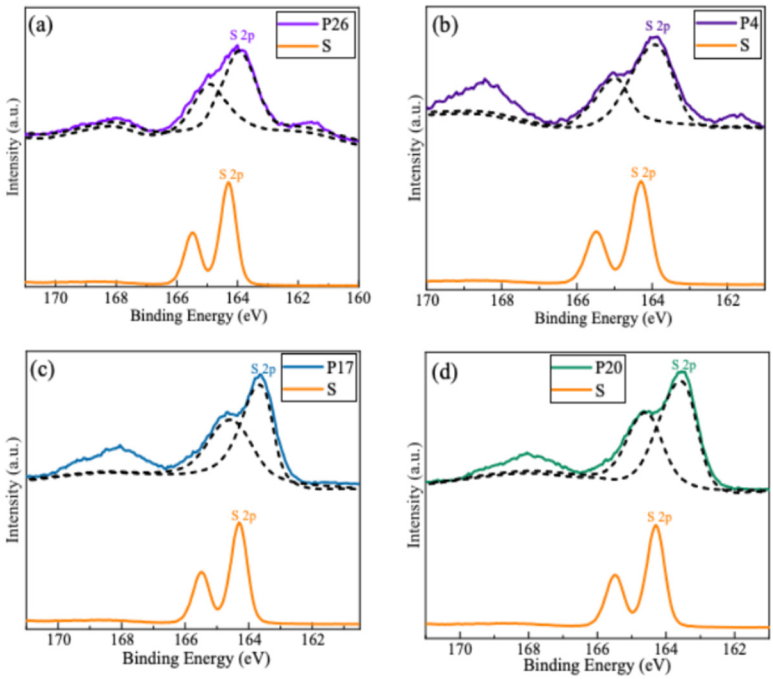

Figure 5. XPS analysis of the S 2p orbital of polythioamide.

Elemental analysis was carried out on selected polysulfonamide samples using an EA3000 organic elemental analyzer (Figure 6). The sulfur content was found to range from 15% to 35%, demonstrating that sulfur was effectively incorporated into the polymer backbone during synthesis. This incorporation confirms the success of the designed synthetic route and provides direct evidence of sulfur embedding within the polymeric framework.

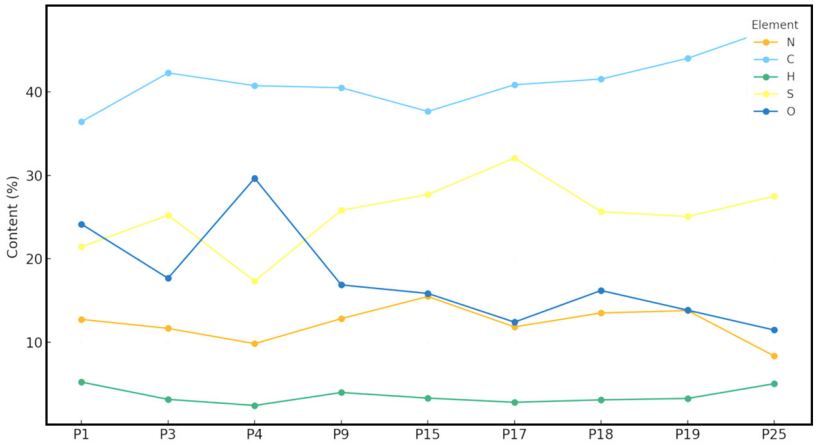

Figure 6. Proportion of each organic element content of polythioamide.

2.5. TG Analysis

Polyamides (commonly known as nylons) are thermoplastic resins with repeating amide groups "-(C=O)NH-" in the polymer backbone. They are widely recognized for their low density, high mechanical strength, excellent toughness, and thermal resistance, and are typically supplied as cylindrical pellets with molecular weights of 15,000–20,000 for plastic applications. Consistent with the literature [38–40], polyamides also exhibit good flame retardancy and very high tensile strength

© 2025 by the author(s). Distributed under a Creative Commons CC BY license.

Preprints.org (www.preprints.org) | NOT PEER-REVIEWED | Posted: 25 November 2025 doi:10.20944/preprints202511.1916.v1

(up to 104 MPa). In this study, a key modification was the replacement of oxygen atoms with sulfur in the backbone. This result indicates that the reaction of sulfur with acids and amines produces true polymeric structures rather than simple physical mixtures, highlighting the robustness of the polymerization method.

Attributed to the presence of extensive inter- and intramolecular hydrogen bonding in polythioamide, it exhibits good thermal stability. Figure 7a presents the weight loss curves for selected polythioamide products, using six materials as examples. P1, P8, P23, and P25 are aliphatic polythioamides, while P17 and P18 are aromatic polythioamides. As shown in the Figure 7a, the temperature range for a 5% weight loss ($T_{5\%}$) falls between 146 °C and 168 °C. The temperature at which the maximum weight loss rate occurs (T_{max}) ranges from 500 °C to 600 °C, and the temperature range at complete weight loss (T_{over}) is between 617 °C and 650 °C. Additionally, there is no significant difference in the weight loss rate and the temperature range corresponding to proportional weight loss between aliphatic and aromatic polythioamides.

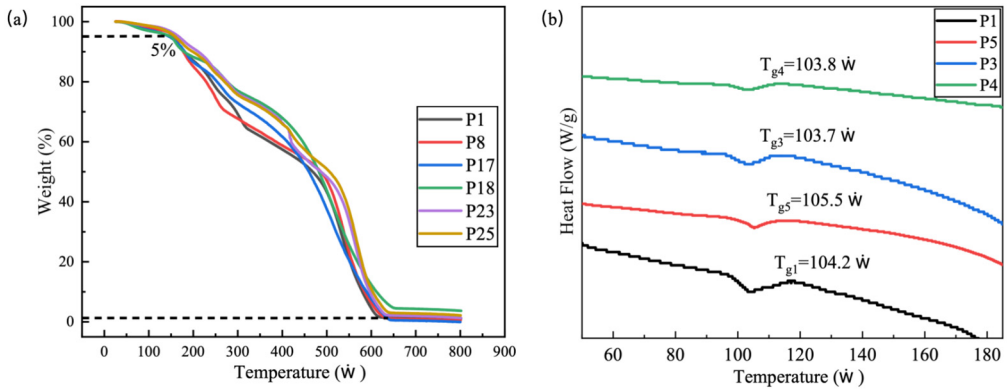

Figure 7. (a) TGA curve of P1, P8, P17, P18, P23, P25 (Test condition: air atmosphere, 10 ℃/min),**(b)** DSC curve of P1, P5, P3, P4, (Test condition: N2 atmosphere, 10 ℃/min).

On the other hand, polythioamides synthesized from different monomer structures showed no significant differences in glass transition temperature (Tg), which remained within the range of 100–110 °C (Figure 7b). Among them, the aliphatic polythioamides P1 and P5 exhibited slightly higher Tg values than the aromatic polythioamides P3 and P4.

2.6. Adsorption of Hg(II) from Aqueous Solution

The adsorption behavior of polythioamides P1–P26 toward Hg(II) was evaluated, and the results are summarized in (Figure 8). Experiments were carried out using 10 mg of adsorbent with an initial Hg(II) concentration (C_0) of 100 mg·L^{-1} and a contact time of 1 h. The adsorption efficiencies were calculated based on the standard equation.

Adsorption Efficiency (η):

$$\eta = \frac{(C_0 - C_e)}{C_0} \times 100\% \quad \text{or} \quad \eta = \frac{(A_0 - A_e)}{A_0} \times 100\%$$

where:

η is the adsorption efficiency (%),

A_0 is the initial absorbance of Hg(II),

A_e is the absorbance of Hg(II) after adsorption.

As shown in the figures, most polythioamides achieved adsorption efficiencies exceeding 90%, while a few samples exhibited relatively lower values. Interestingly, the structural differences between aliphatic and aromatic polythioamides did not significantly influence their performance, indicating that the adsorption of Hg(II) is largely independent of backbone type. This result highlights the structural universality of polythioamides in mercury removal, as both aliphatic and

© 2025 by the author(s). Distributed under a Creative Commons CC BY license.

Preprints.org (www.preprints.org) | NOT PEER-REVIEWED | Posted: 25 November 2025 doi:10.20944/preprints202511.1916.v1

aromatic variants demonstrated consistently high adsorption efficiencies. Such findings suggest that polythioamides are promising adsorbents with broad applicability for the removal of Hg(II) from aqueous environments.

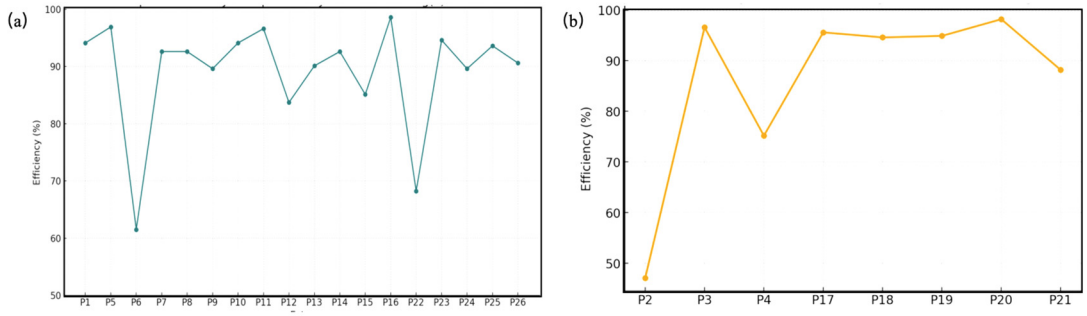

Figure 8. (a) Adsorption efficiency of aliphatic polythioamides for Hg(Ⅱ) in water, **(b)** Adsorption efficiency of aromatic polythioamides for Hg(Ⅱ) in water.

2.7. Characterization of Polythioamides After Hg(II) Adsorption – SEM Analysis

The morphological changes of polythioamides before and after Hg(II) adsorption were investigated by scanning electron microscopy (SEM), as shown in Figure 9. The aliphatic polythioamides P13 and P14 exhibited distinct alterations in surface structure upon adsorption. For P13, the pristine material showed a surface free of pores but containing wrinkles and protrusions. After Hg(II) adsorption, layered aggregation became evident, and the protrusions increased markedly. In contrast, the surface of P14 appeared smooth with few protrusions before adsorption, whereas distinct wrinkles and surface irregularities developed after adsorption.

These morphological transformations suggest that Hg(II) ions were effectively captured and immobilized on the polysulfonamide surfaces. The formation of wrinkles, protrusions, and layered aggregates indicates strong interactions between Hg(II) and the polymer matrix, which may involve coordination with functional groups or surface complexation. Such changes provide direct microscopic evidence supporting the high adsorption efficiency of polythioamides toward Hg(II).

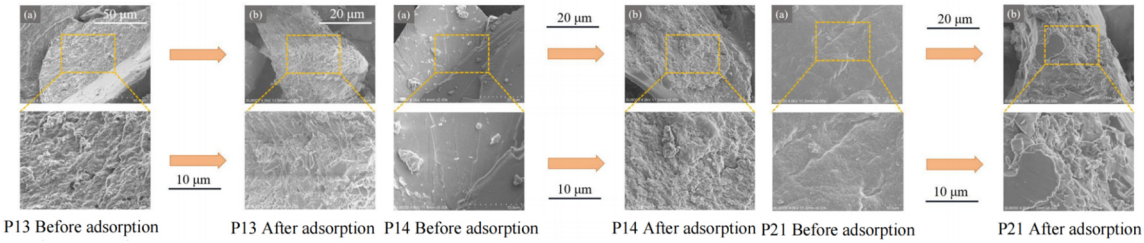

Figure 9. SEM images of P13, P14, P21 before and after adsorption of Hg(II).

2.8. Characterization of Polythioamides After Hg(II) Adsorption (XPS) Analysis

The XPS spectra of polysulfonamide P17 after Hg(II) adsorption are presented in Figure 10. Distinct S 2p and Hg 4f core-level peaks were observed, confirming the presence of sulfur and mercury on the material surface. The S 2p peak appeared at 163.60 eV, which represents a shift from 164.00 eV in the pristine sample. This decrease in binding energy indicates that Hg(II) adsorption alters the electronic environment of sulfur, demonstrating a significant interaction between Hg(II) ions and the polymer matrix.

The Hg 4f spectrum displayed typical spin–orbit splitting, with doublet peaks at 101.80 eV (4f7/2) and 104.80 eV (4f5/2). Both values are higher than those reported for Hg(II) species (100.2 eV and 103.9 eV, respectively). Such a positive shift can be attributed to strong coordination between Hg(II)

© 2025 by the author(s). Distributed under a Creative Commons CC BY license.

Preprints.org (www.preprints.org) | NOT PEER-REVIEWED | Posted: 25 November 2025 doi:10.20944/preprints202511.1916.v1

ions and sulfur-containing functional groups in the polymer. The formation of stable coordination bonds leads to electron density redistribution around the Hg centers, thereby increasing their binding energy.

Taken together, these results provide compelling evidence for the formation of S–Hg coordination bonds during the adsorption process. Moreover, no impurity peaks were detected in the spectra, confirming the absence of external interference and ensuring the reliability of the experimental results.

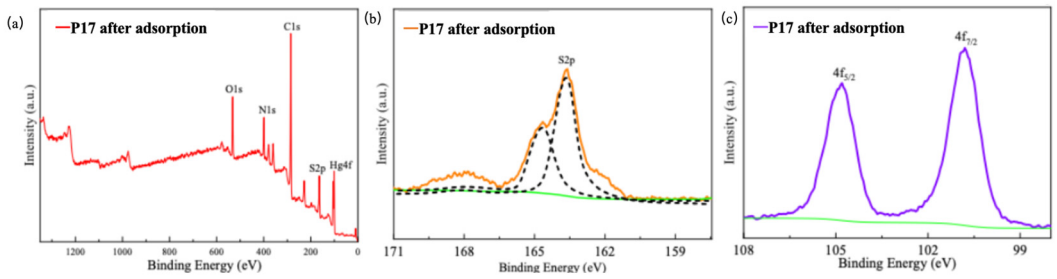

Figure 10. XPS Analysis of P17 after the adsorption of Hg(II).

2.9. Polymerization Mechanism Verification

To elucidate the polymerization mechanism, polythioamide synthesis was investigated using P1 as a representative example. The reactions among elemental sulfur (S_8), dicarboxylic acid (2c), and diamine (3a or 3b) were conducted under identical conditions to identify the source of sulfur and clarify the reaction pathways. As shown in Figure 11a, the mixture of dicarboxylic acid (2c) and diamine (3a) produced the corresponding salt, which appeared as a white solid insoluble in DMSO but soluble in water. In contrast, no apparent reaction occurred between elemental sulfur and dicarboxylic acid, indicating that the sulfur atoms incorporated in the final polymer originate from elemental sulfur rather than from the solvent. When elemental sulfur was heated with diamine (3b) at 100 °C, the color of the system gradually turned deep orange, suggesting the formation of polysulfide intermediates via S_8 ring-opening reactions.

Based on the experimental results and literature analysis, a plausible reaction mechanism is proposed (Figure 11b). Initially, S_8 undergoes nucleophilic attack by amine groups, leading to the formation of linear polysulfide chains with active sulfur radicals. Simultaneously, the carboxylic acid reacts with the amine via a proton transfer process, forming amide intermediates and releasing water or CO_2. Subsequently, the thiol or thioamide intermediates interact with polysulfide radicals, generating reactive intermediate A. Under the influence of fatty diamines, intermediate A undergoes further condensation to form intermediate B, which is then structurally rearranged to produce thioamide-containing polymer chains. The final condensation step results in the formation of cross-linked polythioamide networks, as illustrated in Figure 11b.

This mechanistic pathway suggests that the polymerization proceeds through a stepwise process involving S_8 ring opening, amine nucleophilic substitution, and thioamide bond formation. The presence of diamines plays a crucial role in maintaining sufficient nucleophilic reactivity and in driving the formation of extended conjugated thioamide structures, leading to the characteristic dark-colored product observed experimentally.

© 2025 by the author(s). Distributed under a Creative Commons CC BY license.

Preprints.org (www.preprints.org) | NOT PEER-REVIEWED | Posted: 25 November 2025 doi:10.20944/preprints202511.1916.v1

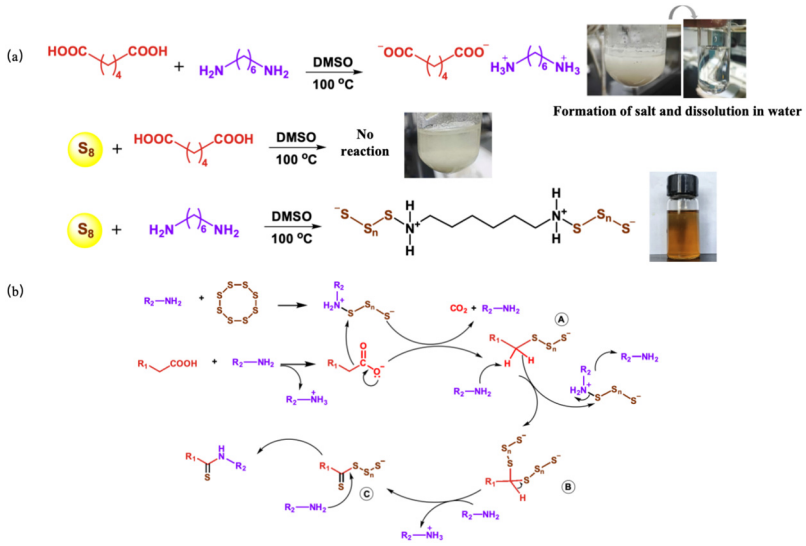

Figure 11. (a) The experimental phenomena and results of the pairwise reactions among elemental sulfur, dicarboxylic acid, and diamine. **(b)** Schematic diagram of the feasible mechanisms of elemental sulfur, carboxylic acids, and amines.

3. Experiment

3.1. Materials and Methods

The chemical reagents used in this study are of analytical grade, and no additional purification was performed. The specific reagents and their sources are as follows: Sublimed sulfur, adipic acid, 1,4-phenylenediacetic acid, succinic acid, glutaric acid, suberic acid, azelaic acid, and sebacic acid were obtained from Sigma-Aldrich (St. Louis, MO, USA) and used without further purification. Diamines, including hexamethylenediamine, putrescine (1,4-butanediamine), p-phenylenediamine, 1,2-propylenediamine, and 1,3-propylenediamine, were used as received.

Main instruments: X-ray diffractometer (XRD), Rigaku D/MAX-2500 (Rigaku Corporation, Tokyo, Japan), used for characterizing the structure. X-ray photoelectron spectroscopy (XPS), PHI 5000 (Physical Electronics, Chanhassen, MN, USA), was used to analyze the sample's surface chemical state. Thermogravimetric analyzer (TGA), Shimadzu DTG-60 (Shimadzu Corporation, Kyoto, Japan),SEM analysis was performed using a Hitachi SU8010 field emission scanning electron microscope. The samples were coated with a thin layer of gold before imaging, and the images were captured at an accelerating voltage of 15 kV.

3.2. Synthesis of Polythioamides

The synthesis of polymers P1–P26 (Figure 12) was conducted using elemental sulfur, diacids, and diamines as monomers. Two representative procedures are described below for the preparation of aliphatic and aromatic polythioamides.

Synthesis of Aliphatic Polythioamide (P1)

Polymer P1 was synthesized from elemental sulfur, adipic acid, and hexamethylenediamine. In a 50 mL polymerization tube, sublimed sulfur (256.0 mg, 8 mmol), adipic acid (584.5 mg, 4 mmol), and hexamethylenediamine (232.4 mg, 2 mmol) were combined, followed by 10 mL of DMSO as the reaction solvent. The mixture was stirred continuously at 100 °C for 15 h. After cooling to room temperature, the solution was slowly dropped through cotton into 300 mL of ethanol stirred at 500 rpm to precipitate the polymer. The solid was filtered, thoroughly washed with ethanol (5 × 20 mL), and dried to yield a black product (P1) with a yield of 61%.

© 2025 by the author(s). Distributed under a Creative Commons CC BY license.

Preprints.org (www.preprints.org) | NOT PEER-REVIEWED | Posted: 25 November 2025 doi:10.20944/preprints202511.1916.v1

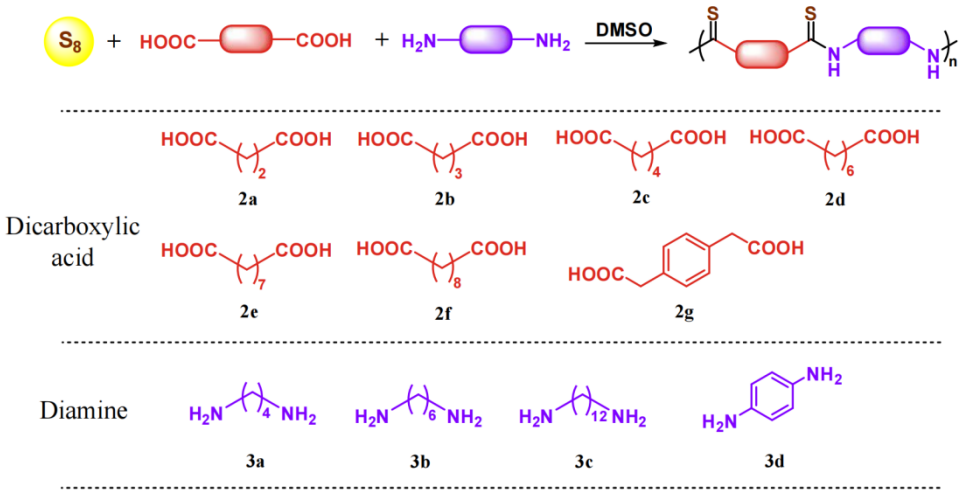

Figure 12. Structures of the seven diamine monomers and four dicarboxylic acid monomers used for the synthesis of polythioamides, along with their corresponding reaction equations.

Synthesis of Aromatic Polythioamide (P17)

Polymer P17 was synthesized from elemental sulfur, succinic acid, and p-phenylenediamine. Sublimed sulfur (256 mg, 8 mmol), succinic acid (472.4 mg, 4 mmol), and p-phenylenediamine (216.3 mg, 2 mmol) were placed in a 50 mL polymerization tube, followed by 10 mL of DMSO. The mixture was stirred at 100 °C for 15 h. After cooling to room temperature, 20 mL of DMF was added to dissolve and dilute the crude product. The solution was then slowly dropped through cotton into 300 mL of ethanol stirred at 500 rpm to precipitate the polymer. The precipitate was filtered, thoroughly washed with ethanol (5 × 20 mL), and dried to obtain the final black polymer (P17) with a yield of 93%. The synthetic process is illustrated in Figure 13.

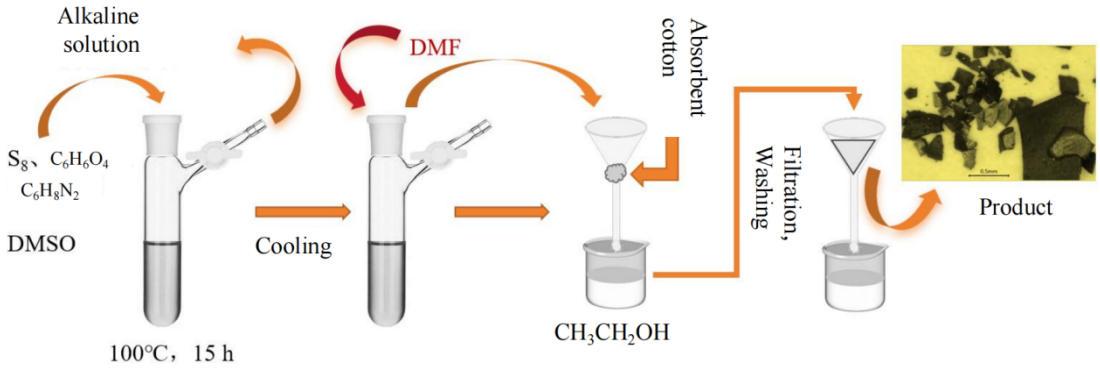

Figure 13. Synthesis process of polythioamide.

3.3. Adsorption Performance of Polythioamides

Hg(II) Adsorption by polythioamides

The adsorption performance of polythioamides toward Hg(II) was systematically investigated. As a representative example, polymer P1 was tested under standard conditions. Specifically, 10 mg of P1 was dispersed in 100 mg·L^{-1} Hg(II) solution in a 20 mL tube and stirred magnetically at room temperature for 1 h. The suspension was centrifuged at 4000 rpm for 5 min, and the supernatant was filtered through a 0.22 μm membrane to obtain the final solution for analysis. Aliquots of the filtrate were mixed with KI–ascorbic acid, PVA, and Rhodamine B solutions, diluted to 50 mL, and the absorbance was measured at 598 nm. The adsorption capacity and efficiency were calculated using standard equations.

To assess the general performance of the materials, adsorption experiments were conducted for polymers P1–P26 using the same initial Hg(II) concentration (100 mg·L^{-1}).

© 2025 by the author(s). Distributed under a Creative Commons CC BY license.

Preprints.org (www.preprints.org) | NOT PEER-REVIEWED | Posted: 25 November 2025 doi:10.20944/preprints202511.1916.v1

Characterization of Adsorbent Materials

Polymer P1 was further characterized after Hg(II) adsorption to explore the underlying adsorption mechanism. Field-emission scanning electron microscopy (FE-SEM) revealed significant morphological changes, including increased surface roughness and the formation of layered aggregates, which are consistent with Hg(II) deposition on the polymer surface. X-ray photoelectron spectroscopy (XPS) confirmed the presence of both sulfur and mercury signals, with shifts in S 2p and Hg 4f binding energies. These shifts provide strong evidence for the formation of coordination bonds between Hg(II) and sulfur-containing functional groups within the polymer matrix. The redistribution of electron density associated with this coordination explains the enhanced binding energies observed in the XPS spectra.

Adsorption Isotherm Model

The adsorption isotherm model is an essential theoretical tool for understanding the equilibrium relationship between the adsorbate concentration in solution and the amount adsorbed on the adsorbent surface. In this study, the adsorption behavior of Hg(II) ions on polythioamide materials was analyzed using the Langmuir isotherm models. The Langmuir model assumes a homogeneous adsorption surface with identical binding sites, uniform adsorption energies, and monolayer adsorption without interaction between adsorbed molecules. The linearized form of the Langmuir equation is expressed as:

$$\frac{C_e}{q_e} = \frac{1}{q_m K_L} + \frac{C_e}{q_m}$$

where C_e (mg·L^{-1}) is the equilibrium concentration of Hg(II), q_e (mg·g^{-1}) is the equilibrium adsorption capacity, K_L (L·mg^{-1}) is the Langmuir adsorption constant, and q_m (mg·g^{-1}) represents the maximum adsorption capacity.

As shown in Figure 14, the plot of C_e/q_e versus C_e for the adsorption of Hg(II) on polythioamide P1 exhibits a high degree of linearity with a correlation coefficient R^2=0.99157. The linear fitting equation, y=0.00511x+0.06178, indicates excellent agreement with the Langmuir model, suggesting that the adsorption process is dominated by monolayer chemisorption on a uniform surface. This result confirms that the binding sites on P1 possess similar affinity toward Hg(II) ions and that surface saturation occurs once a monolayer is formed.

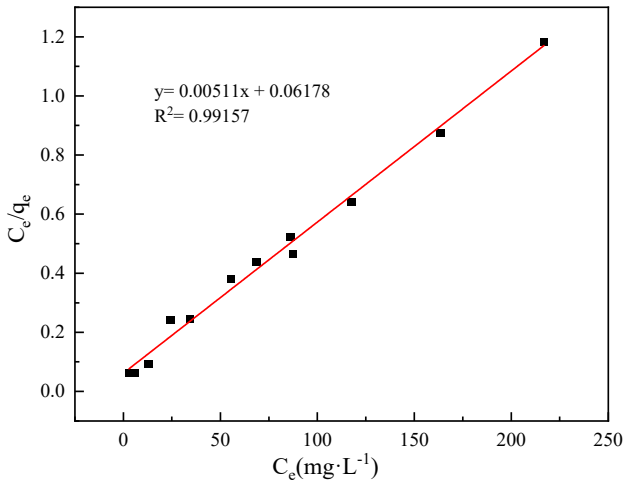

Figure 14. Diagram of the relationship between Ce and qe of P1 adsorbed Hg(Ⅱ).

Effect of Experimental Conditions

The influence of environmental factors on adsorption performance was systematically evaluated. Parameters including temperature, pH, contact time, initial Hg(II) concentration, and the

© 2025 by the author(s). Distributed under a Creative Commons CC BY license.

Preprints.org (www.preprints.org) | NOT PEER-REVIEWED | Posted: 25 November 2025 doi:10.20944/preprints202511.1916.v1

presence of competing ions were varied. These findings indicate that Hg(II) adsorption by polythioamides is spontaneous.

The effect of different adsorbent dosages on the adsorption of Hg(II) in water

Figure 15a. This figure shows the effect of varying the amount of the polythioamide P1 on the Hg(II) adsorption efficiency in water. As shown in the figure, the Hg(II) adsorption efficiency increases steadily with the increasing dosage of P1. This trend is primarily due to the linear increase in the number of active adsorption sites on the surface of the adsorbent. Notably, when the amount of P1 is increased from 8 mg to 10 mg, the Hg(II) adsorption efficiency rises significantly from 83.05% to 94.08%. However, further increases in the P1 dosage to 15 mg and 20 mg only lead to minimal improvements in efficiency (1.2% and 0.4%, respectively), indicating that the adsorption process reaches saturation at these concentrations.

The effect of different pH values on the polymer's adsorption of Hg(II) in water

We have included the data for the influence of pH on the Hg(II) adsorption performance of the polythioamide material P1, which is presented in Figure 15b. The experimental data show that the Hg(II) adsorption efficiency decreases as the pH increases. This is primarily due to the hydrolysis equilibrium of Hg(II) in the solution: as the pH rises, Hg(II) is converted into $Hg(OH)_2$ precipitate, with a solubility product constant of $Ksp(Hg(OH)_2) = 3.0\times10^{-}25$. In strongly acidic conditions (pH < 3), this hydrolysis process is effectively suppressed.

The results indicate that the material exhibits excellent adsorption performance at pH = 1.0 and 2.0, confirming the material's structural stability and high adsorption capacity in strongly acidic media. However, the differences between pH = 1.0 and pH = 2.0 were not significant. Considering factors such as cost and environmental friendliness, pH ≈ 2 was selected as the optimal condition for subsequent Hg(II) adsorption studies.

The effect of different temperatures on the polymer's adsorption of Hg(II) in water

Figure 15c illustrates the impact of temperature on the Hg(II) adsorption performance of the polythioamide P1.

As shown in the figure, when the initial Hg(II) concentration is 100 $mg\cdot L^{-1}$, the adsorption efficiency increases from 94.08% at 25 °C to 98.90% at 50 °C. This increase in efficiency with rising temperature suggests that the adsorption process is endothermic, and higher temperatures promote the adsorption reaction.

Given that the material already demonstrated excellent adsorption performance in a strongly acidic environment at room temperature (25 °C) with an adsorption efficiency of 94.08%, further increases in temperature resulted in only a modest improvement of 4.82%. Considering the simplicity of experimental operations and the economic aspects of energy consumption, we selected 25 °C as the standard reaction temperature for subsequent experiments.

The effect of different initial Hg(II) concentrations on the polymer's adsorption performance.

Figure 15d illustrates the impact of varying Hg(II) initial concentration on the adsorption performance.

The experimental results show two significant trends as the Hg(II) concentration increases from low to high (up to 400 $mg\cdot L^{-1}$). First, the adsorption capacity per unit increases and reaches a peak (187.7 $mg\cdot g^{-1}$) in the concentration range of 250–275 $mg\cdot L^{-1}$. Second, once the Hg(II) concentration exceeds 275 $mg\cdot L^{-1}$, the adsorption efficiency starts to decline. This seemingly contradictory behavior is explained by the competition between adsorption kinetics and thermodynamics: at lower concentrations (<250 $mg\cdot L^{-1}$), the mass transfer process driven by concentration gradients dominates, leading to a rapid increase in adsorption. However, when the initial concentration exceeds 275 $mg\cdot L^{-1}$, the active sites on the material surface become saturated, and while the concentration continues to increase, the adsorption capacity stabilizes, indicating that the maximum adsorption capacity of the material has been reached.

Based on this analysis, we have also tested the maximum adsorption capacity for the products with good adsorption efficiency (over 80%) from the 26 synthesized products. The results are provided in Figure 15e.

© 2025 by the author(s). Distributed under a Creative Commons CC BY license.

Preprints.org (www.preprints.org) | NOT PEER-REVIEWED | Posted: 25 November 2025 doi:10.20944/preprints202511.1916.v1

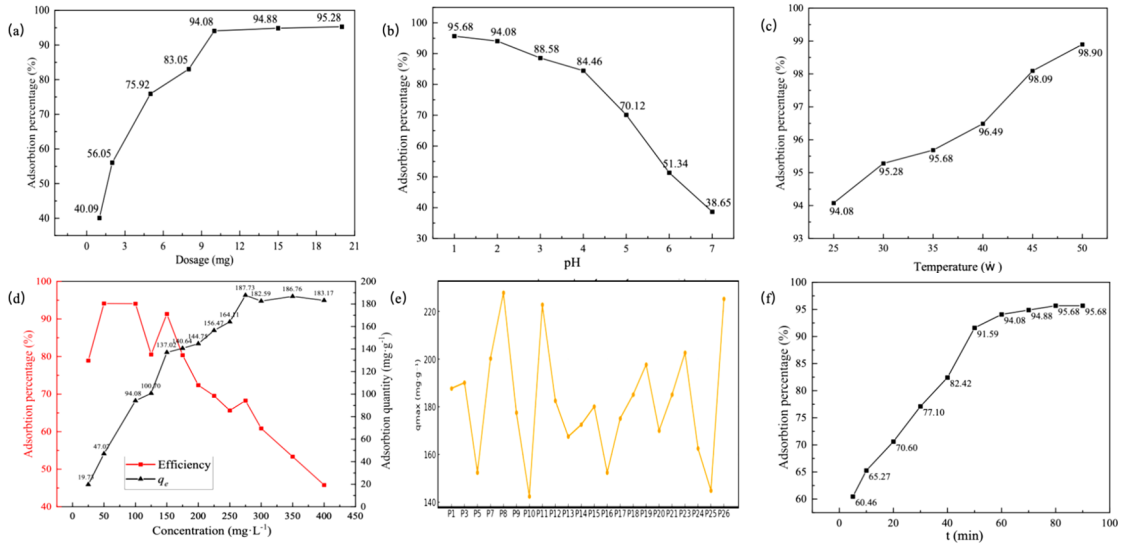

Figure 15. (a) Effect of dosage of polythioamide P1 on Hg(Ⅱ) adsorption in water (C_0=100 mg·L^{-1}, T=25 °C, V=10 mL), **(b)** Effect of pH on the effect of adsorption of Hg(Ⅱ) by polythioamide (C_0=100 mg·L^{-1}, T=25 ℃, V=10 mL), **(c)** Effect of temperature on the effect of polythioamide on the adsorption of Hg(Ⅱ) in water, **(d)** Hg(Ⅱ) adsorption properties of polythioamide at different initial Hg(Ⅱ) concentrations (T=25 ℃, V=10 mL), **(e)** Maximum adsorption capacity of polythioamide, **(f)** Relationship between adsorption efficiency of polythioamide P1 adsorbed Hg(II) over time.

The effect of different contact times on the polymer's adsorption of Hg(II) in water.

Figure 15f presents the relationship between adsorption efficiency and contact time, revealing the dynamic effect of time on adsorption efficiency.

As shown in the figure, the material exhibits rapid adsorption characteristics at the beginning of the reaction. Within just 5 minutes, the Hg(II) adsorption efficiency exceeds 60%. After 50 minutes, the adsorption efficiency increases further to over 90%, but the rate of adsorption slows down. When the reaction time is extended from 60 to 90 minutes, the increase in adsorption efficiency is less than 2%, indicating that the adsorption process has approached equilibrium.

The adsorption process of polythioamide for Hg(II) in water shows clear stages. During the first 0–60 minutes, the material's surface contains many unoccupied active sites, and the strong acidic environment (pH ≈ 2) helps promote the adsorption process, leading to a rapid increase in Hg(II) adsorption efficiency. After 60 minutes, the adsorption curve levels off, and the adsorption efficiency stabilizes because the active sites on the material's surface are nearly saturated. At this point, extending the reaction time provides limited additional benefit.

Considering both adsorption kinetics and practical efficiency, we determined that 60 minutes is the optimal adsorption time for this study.

4. Conclusions

In this study, a catalyst-free one-pot multicomponent polymerization strategy was developed to achieve the dual goals of high-value utilization of industrial waste sulfur and remediation of mercury pollution. Using elemental sulfur, dicarboxylic acids, and diamines as monomers, 26 structurally tunable polythioamides were successfully synthesized in high yields (>92%) under mild conditions.

The resulting polythioamides exhibited outstanding Hg(II) adsorption performance, with removal efficiencies exceeding 90%. It revealed that aromatic amine units contributed more significantly to Hg(II) adsorption than diacid units, and longer aliphatic amine chains enhanced adsorption capacity.

© 2025 by the author(s). Distributed under a Creative Commons CC BY license.

Preprints.org (www.preprints.org) | NOT PEER-REVIEWED | Posted: 25 November 2025 doi:10.20944/preprints202511.1916.v1

Overall, this work not only provides a sustainable pathway for the valorization of industrial waste sulfur but also introduces a new class of highly effective Hg(II) adsorbents. These findings highlight the potential of polythioamides for practical applications in environmental remediation and mercury pollution control.

Author Contributions: Material preparation, catalytic experiments and writing—original draft, Y.G.; writing—review & editing, C.M.; data analysis, X.Q., H.Y.; theoretical investigation, J.Z., W.X.; original idea and supervision, C.Y., H.D. All authors have read and agreed to the published version of the manuscript.

Funding: The study was supported by the university-level team research project of Sinopec Science and Technology Department Project: Fundamental Research on the Synthesis of Functional High-Sulfur Polymers (224072); Hainan Vocational University of Science and Technology in 2024 "Research on Polyionic Liquid Materials and Their Catalytic Properties (HKKY2024-TD-17)"; Hainan Province 2025 Higher Education Teaching Reform Research Project: Research on the Ideological and Political Teaching Model of the "Principles of Chemical Engineering" Course Based on Target Problem-Oriented Approach (Hnjg2025ZC-127), Hainan Province 2025 Higher Education Scientific Research Project: Study on Polyionic Liquid Materials and Their Photocatalytic Performance (Hnky2025-66), Research on Teaching Methods of Mechanical Manufacturing Courses under Informationization Conditions (HKJG2024-35). The Hainan University of Science and Technology Vocational College Innovation and Entrepreneurship Training Program for College Students also provided support (2025).

Data Availability Statement: The data that support the findings of this study are available from the corresponding author upon reasonable request.

Conflicts of Interest: The authors declare no conflict of interest.

References

1. Kutney, G. Sulfur: History, Technology, Applications and Industry; Elsevier: 2023.
2. Ibrahim, A. Y.; Elgazzar, M.; Abdelkhalik, A.; et al. Performance Assessment and Process Optimization of a Sulfur Recovery Unit: A Real Starting-Up Plant. Environ. Monit. Assess. 2023, 195, 358.
3. Haghighatjoo, F.; Ghorbani, A.; Rahimpour, M. R. Sulfur Recovery from Natural Gas. Adv. Nat. Gas: Form., Process., Appl. 2024, 7, 247–262.
4. Ghumman, A. S. M.; et al. Evaluation of Properties of Sulfur-Based Polymers Obtained by Inverse Vulcanization: Techniques and Challenges. Polym. Polym. Compos. 2021, 29, 1333–1352.
5. Discekici, E. H.; et al. Evolution and Future Directions of Metal-Free Atom Transfer Radical Polymerization. Macromolecules 2018, 51, 7421–7434.
6. Zheng, B.; et al. Emerging Functional Porous Polymeric and Carbonaceous Materials for Environmental Treatment and Energy Storage. Adv. Funct. Mater. 2020, 30, 1907006.
7. Amna, R.; Alhassan, S. M. A Comprehensive Exploration of Polysulfides, from Synthesis Techniques to Diverse Applications and Future Frontiers. ACS Appl. Polym. Mater. 2024, 6, 4350–4377.
8. Alsolami, E. S.; et al. One-Pot Multicomponent Polymerization Towards Heterocyclic Polymers: A Mini Review. RSC Adv. 2024, 14, 1757–1781.
9. Li, Q. R.; et al. A Strategy to Develop Hydrophobic Stainless Steel Mesh through Three-Component Coupling Reaction with Presence of Sulfur. Surf. Interfaces 2023, 42, 103427.
10. Brirmi, N. E. H.; et al. Progress and Challenges in Heterocyclic Polymers for the Removal of Heavy Metals from Wastewater: A Review. Water Emerg. Contam. Nanoplastics 2024, 3, N-A.
11. Zhao, J. Z.; Yue, T. J.; Ren, B. H.; Lu, X. B.; Ren, W. M. Closed-Loop Recycling of Sulfur-Rich Polymers with Tunable Properties Spanning Thermoplastics, Elastomers, and Vitrimers. Nat. Commun. 2024, 15, 3002.
12. Ma, S.; et al. One-Pot Synthesis of Fluorescent Guanidyl Sulfur Quantum Dots for Antibacterial and Antioxidant Performance. ACS Appl. Nano Mater. 2025, 8, 4580–4590.
13. Stiernet, P.; Debuigne, A. Imine-Based Multicomponent Polymerization: Concepts, Structural Diversity and Applications. Prog. Polym. Sci. 2022, 128, 101528.

© 2025 by the author(s). Distributed under a Creative Commons CC BY license.

Preprints.org (www.preprints.org) | NOT PEER-REVIEWED | Posted: 25 November 2025 doi:10.20944/preprints202511.1916.v1

14. Yue, T.-J.; Ren, W.-M.; Lu, X.-B. Copolymerization Involving Sulfur-Containing Monomers. Chem. Rev. 2023, 123, 14038–14083.
15. Chen, X.; Qin, A.; Tang, B. Z. Green Synthesis of Sulfur-Containing Polymers by Carbon Disulfide-Based Spontaneous Multicomponent Polymerization. Green Chem. 2024, 26, 857–865.
16. Li, S.; et al. Metal-Free Multicomponent Polymerization to Access Polythiophenes from Elemental Sulfur, Dialdehydes, and Imides. Polym. Chem. 2025. (in press)
17. Huang, Y.; Hu, R.; Tang, B. Z. Multicomponent Polymerization of Sulfur, Diynes, and Aromatic Diamines and Facile Tuning of Polymer Backbone Structures. Macromolecules 2024, 57, 6568–6576.
18. Aarsen, C. V.; et al. Designed to Degrade: Tailoring Polyesters for Circularity. Chem. Rev. 2024, 124, 8473–8515.
19. Junyao; et al. Catalyst-Free Synthesis of Diverse Fluorescent Polyoxadiazoles for the Facile Formation and Morphology Visualization of Microporous Films and Cell Imaging. Chem. Sci. 2023, 14, 903–915.
20. Rao.; Chen, Q. Thio-Groups Decorated Covalent Triazine Polyamide (TTPA) for Hg2+ Adsorption: Efficiency and Mechanism. J. Environ. Chem. Eng. 2024, 12, 112340.
21. Chaoji; et al. Novel Triazine-Based Sulfur-Containing Polyamides: Preparation, Adsorption Efficiency and Mechanism for Mercury Ions. Eur. Polym. J. 2024, 202, 112588.
22. Guo, Z.; Chen, Y.; Jiang, B.; Ye, S.; Yi, W. Functional Polythioamides Derived from Thiocarbonyl Fluoride. Angew. Chem. 2023, 135, e202313779.
23. Gao, Y.; Cao, T.; Du, J.; et al. The Bi-Modified (BiO)2CO3/TiO2 Heterojunction Enhances the Photocatalytic Degradation of Antibiotics. Catalysts 2025, 15, 56.
24. Ding, R.; et al. Sulfhydryl Functionalized Chitosan-Covalent Organic Framework Composites for Highly Efficient and Selective Recovery of Gold from Complex Liquids. Int. J. Biol. Macromol. 2024, 282, 137037.
25. Pasadakis, N.; Livanos, G.; Zervakis, M. Deconvolving the Absorbance of Methyl and Methylene Groups in the FT-IR 3000–2800 cm-Band of Petroleum Fractions. Spectroscopy 2013, 10, 25–35.
26. Thombare, N.; et al. Comparative FTIR Characterization of Various Natural Gums: A Criterion for Their Identification. J. Polym. Environ. 2023, 31, 3372–3380.
27. Leewis, C. M.; et al. Ammonia Adsorption and Decomposition on Silica Supported Rh Nanoparticles Observed by in Situ Attenuated Total Reflection Infrared Spectroscopy. Appl. Surf. Sci. 2006, 253, 572–580.
28. Basir, N. F. A.; et al. Synthesis and Characterization of 5-Cyclopentylsulfanyl-3H- [1,3,4] Thiadiazole-2-Thione and Study of Its Single-Crystal Structure, FTIR Spectra, Thermal Behavior, and Antibacterial Activity. J. Therm. Anal. Calorim. 2024, 149, 10745–10756.
29. Cao, M.; et al. Effect of Elemental Sulfur (S8) on Carbon Isotope Analysis of n-Alkanes. Geochem. Int. 2023, 61, 1155–1163.
30. Liu, Y.; et al. Laser Microprobe Technique for Stable Carbon Isotope Analyses of Organic Carbon in Sedimentary Rocks. Geochem. J. 2000, 34, 195–205.
31. Cai, D. Syntheses of Sulfur Rich Polymers and Their Application in Heavy Metal Capture. Ph.D. Thesis, University of Liverpool, 2025.
32. Amna, R. Sulfur Copolymers via Emulsion Polymerization. Ph.D. Thesis, Khalifa University of Science, 2023.
33. Huang, D.; et al. Minute-Scale Evolution of Free-Volume Holes in Polyethylenes During the Continuous Stretching Process Observed by in Situ Positron Annihilation Lifetime Experiments. Macromolecules 2023, 56, 4748–4759.
34. Demleitner, M.; et al. Influence of Block Copolymer Concentration and Resin Crosslink Density on the Properties of UV-Curable Methacrylate Resin Systems. Macromol. Mater. Eng. 2022, 307, 2200320.
35. Yang, Y.; et al. Mechanisms and Effects of Sunlight Exposure on Disperse-Dyed Aromatic Polysulfonamide Fibers. Surface Innov. 2025, 13, 176–186.
36. Li, Q.; et al. High Rejection Seawater Reverse Osmosis TFC Membranes with a Polyamide-Polysulfonamide Interpenetrated Functional Layer. J. Membr. Sci. 2025, 715, 123507.
37. Wang, Z.; et al. Lightweight, Superelastic, and Temperature-Resistant rGO/Polysulfoneamide-Based Nanofiber Composite Aerogel for Wearable Piezoresistive Sensors. J. Mater. Chem. C 2023, 11, 14641–14651.

© 2025 by the author(s). Distributed under a Creative Commons CC BY license.

Preprints.org (www.preprints.org) | NOT PEER-REVIEWED | Posted: 25 November 2025 doi:10.20944/preprints202511.1916.v1

38. Yasin, A.; et al. Hyperbranched Multiple Polythioamides Made from Elemental Sulfur for Mercury Adsorption. Polym. Chem. 2020, 11, 810–819.
39. Akgül, E. T.; et al. Trisurethane Functionalized Sulfonamide Based Polymeric Sorbent: Synthesis, Surface Properties and Efficient Mercury Sorption from Wastewater. Sep. Purif. Technol. 2023, 325, 124606.
40. Hashemi, S. A.; et al. Development of Sulfurized Polythiophene-Silver Iodide-Diethyldithiocarbamate Nanoflakes Toward Record-High and Selective Absorption and Detection of Mercury Derivatives in Aquatic Substrates. Chem. Eng. J. 2022, 440, 135896.

Disclaimer/Publisher's Note: The statements, opinions and data contained in all publications are solely those of the individual author(s) and contributor(s) and not of MDPI and/or the editor(s). MDPI and/or the editor(s) disclaim responsibility for any injury to people or property resulting from any ideas, methods, instructions or products referred to in the content.

© 2025 by the author(s). Distributed under a Creative Commons CC BY license.